# Dynamic State Estimation for Inverter-Based Resources: A Control-Physics Dual Estimation Framework

Heqing Huang, *Student Member, IEEE*, Yuzhang Lin, *Member, IEEE*, Xiaonan Lu, *Senior Member, IEEE*, Yue Zhao, *Member, IEEE*, and Avinash Kumar, *Member, IEEE*

***Abstract*—As Inverter-Based Resources (IBRs) gradually replace conventional synchronous generators (SGs), Dynamic State Estimation (DSE) techniques must be extended for the monitoring of IBRs. The key difference between IBRs and SGs is that the dynamics of IBRs comprise a heavy mix of physical processes and digital controller computations. This paper develops a generic framework of Control-Physics Dynamic State Estimation (CPDSE) for IBRs. First, a control-physics state-space representation of IBRs is presented. Noting the symmetry of the control and physical state spaces, it is proposed to use two dual estimators to track the states of the physical inverter subsystem and the digital controller subsystem, respectively. The CPDSE framework has the capability of suppressing errors in both measurement signals and control signals flowing between the two subsystems and the potential to distinguish between cyber and physical events. The advantages and versatility of the proposed CPDSE framework are validated on a variety of IBR systems (solar, wind, and storage), control strategies (grid-following and grid-forming), and both transmission and distribution systems.**

***Index Terms*—Adaptive cubature Kalman filter, dynamic state estimation, inverter-based resources, grid-forming control, renewable energy, situational awareness.**

## I. Introduction

THE rapid growth of Inverter-Based Resources (IBRs), such as photovoltaics (PV), wind power, and energy storage, is reshaping the dynamic behaviors of power systems [1]. IBRs have significantly different dynamic characteristics than conventional synchronous generators (SGs). Their dynamics are fast, inertia-less [2], distributed, and heavily dependent on their controllers, which are becoming increasingly diverse [3]. IBRs also give rise to new mechanisms of instability, such as wide-band oscillations [2], DC-link voltage transients, and phase-locked loop (PLL) divergence [4]. These differences bring new challenges to various aspects of power system operations, including system modeling, stability analysis [5], protection [6], control [7], and others areas. To address these challenges, IBRs' dynamic behaviors should be better monitored for secure grid operations.

DSE, as a popular monitoring technique, has been extensively investigated for tracking the dynamics of SGs. Common methods include the Extended Kalman Filter (EKF), Unscented Kalman Filter (UKF), Cubature Kalman Filter (CKF), Ensemble Kalman Filter (EnKF), and Particle Filter (PF), just to name a few; and a detailed review can be found in [8].

Despite extensive studies on the DSE of conventional SGs, research on the DSE of IBRs remains relatively unmature. Refs. [9], [10] use UKF and Unscented Particle Filtering for the DSE of Doubly Fed Induction Generator based Wind Turbines (DFIG-WTs). Ref. [11] proposes an EKF with Unknown Inputs to solve the DSE problem for DFIGs with unknown mechanical input torque. Refs. [12], [13] use EKF and EnKF to observe the dynamics of Permanent Magnet Synchronous Generator-based Wind Turbines (PMSG-WTs). An adaptive CKF technique is proposed in [14] for performing DSE of PV generation systems. Ref. [15] propose a DSE framework based on the EKF method combined with consensus control for microgrids containing multiple battery energy storage systems.

Although the DSE for IBRs remains an emerging topic requiring further investigation, it has already inspired many novel applications in the fields of power system modeling, monitoring, control, and protection [16]. Ref. [17] proposes a dynamic modeling method for PMSG wind farm clusters based on an adaptive EKF; a DSE-based fault detection method for switching power inverters is presented in [18]; Ref. [19] proposes a UKF-based frequency estimation and control method using IBRs; a DSE-enabled supplementary predictive control to minimize the transients in IBR-rich systems is presented in [20]; Ref. [21] proposes a DSE-based sliding-mode control (SMC) strategy for DFIG-WTs; DSE-based protection schemes for IBRs and microgrids are developed in [22], [23].

Manuscript received 21 May 2023; revised 11 November 2023; accepted 28 January 2024. Date of publication 6 February 2024; date of current version 21 August 2024. This work was supported in part by National Science Foundation under Award 2143021, in part by the U.S. Department of Energy's Office of Energy Efficiency and Renewable Energy (EERE) under the Solar Energy Technologies Office under Award 38456, and in part by the U.D. Department of Navy inder Award N00014-22-1-2001 issued by the Office of Naval Research. Paper no. TPWRS-00771-2023. *(Corresponding author: Yuzhang Lin.)*

Heqing Huang and Yuzhang Lin are with the Department of Electrical and Computer Engineering, New York University, New York, NY 11201 USA (e-mail: hh3384@nyu.edu; yuzhang.lin@nyu.edu).

Xiaonan Lu is with Purdue University, West Lafayette, IN 47907 USA (e-mail: lu998@purdue.edu).

Yue Zhao is with Electrical and Computer Engineering, Stony Brook University, Stony Brook, NY 11794 USA (e-mail: yue.zhao.2@stonybrook.edu).

Avinash Kumar is with Advanced Research Institute, Virginia Tech, Blacksburg, VA 24060 USA (e-mail: avinashkumar@vt.edu).

Color versions of one or more figures in this article are available at https://doi.org/10.1109/TPWRS.2024.3362701.

Digital Object Identifier 10.1109/TPWRS.2024.3362701

Despite the increasing popularity of DSE for IBRs, the existing methods reviewed above largely follow the DSE paradigm for conventional SGs. However, a critical difference to be noted is that the dynamics of IBRs are heavily dependent on their control strategies. While the state-space models of SGs primarily reflect electro-mechanical processes, a large part of IBR state-space models represent the digital computation of control laws. In other words, the dynamics of IBRs are a heavy mix of physical dynamics and digital dynamics (or control dynamics). Existing research mixes the dynamics of the physical processes with the digital computation of the controller in a single state space, which leads to several essential limitations.

1) As physical states and digital states are blended in a single set of equations, the uncertainties of the two-way data flows between the physical inverter system and the digital controller (i.e., noise and bad data in measurement signals and control signals) cannot be explicitly modeled and filtered.
2) With the blended state-space equations, the change of either inverter physics or control laws will affect all state variables and output signals, resulting in the infeasibility to distinguish between cyber events (e.g., controller failures or attacks) and physical events (e.g., electric circuit faults).
3) The control methods of IBRs are becoming increasingly diverse, such as virtual synchronous generator (VSG) and droop control [24], [25]. For a blended state-space model, the change of control laws will require a thorough modification of the entire DSE model, making it difficult to adapt to the case when IBRs switch between multiple controls during operation.

A possible and reasonable explanation for adopting a blended model in existing research is that the earlier research focus has been primarily on DSE for SGs, and the DSE framework for SGs was naturally adopted by the studies of DSE for IBRs. While the excitation systems or governors of SGs may have controllers, the dynamics at the transient stability time scale are predominantly determined by the physical (electro-mechanical) system. Therefore, the traditional DSE framework for SGs does not involve significant issues of interaction between physical subsystems and control subsystems. For IBRs whose dynamics are a heavy mix of physics and controls, the ignorance of the imperfection and uncertainty in the signal interactions between the physical and control subsystems poses the aforementioned limitations.

In order to address these challenges, we propose a Control-Physics Dynamic State Estimation (CPDSE) framework as a unified DSE paradigm for IBRs. In this framework, we generally divide any IBR system into a physical state space and a control state space, and the interactions between the two subsystems are modeled explicitly. Noting an interesting symmetry between the two subsystems, we develop a dual estimation framework, consisting of a physical DSE and a control DSE, for capturing the states and addressing the uncertainties of the two subsystems, respectively. The main contributions are summarized as follows.

1) A generic CPDSE framework is originally conceptualized, where the control subsystem and the physical subsystem of an IBR are modeled and estimated in a dual structure. It can be applied to arbitrary types of IBRs, allow modeling of data flow uncertainties between the two subsystems, and potentially allow distinguishing between cyber (control) and physical events.
2) An Adaptive CKF (ACKF) algorithm is devised to materialize the proposed CPDSE concept on IBRs with unknown noises of measurements and state transitions. It enables noise filtering and bad data processing for both measurement signals and control signals flowing between the physical and control subsystems.
3) The CPDSE concept and algorithm are validated on a variety of IBRs, including solar PV systems, PMSG-WTs, and battery energy storage systems (BESSs), and a variety of control methods, including Maximum Power Point Tracking (MPPT) grid-following control and VSG grid-forming control, demonstrating the versatility of the proposed framework. Especially, we present interesting results of tracking the virtual "rotor speed" and "power angle" of a VSG, which are controller internal states typically unknown to grid operators.

The rest of the paper is organized as follows. Section II illustrates and discusses the limitations of the traditional blended state-space model for DSE applications and proposes the CPDSE framework. Section III presents an ACKF algorithm to materialize the CPDSE framework for state tracking and bad data processing. Section IV presents comprehensive simulation results of the proposed framework and algorithm in a variety of IBR systems, control strategies, and test systems. Concluding remarks are given in Section V.

## II. Control-Physics State-Space Representation and Dual Dynamic State Estimation Framework

As mentioned in the previous section, an IBR system constitutes a physical subsystem and a control (i.e., digital, or cyber) subsystem. The two subsystems interact with each other through measurement signals and control signals. In this section, we will first show that traditional DSE methods treating the entire IBR as a whole state space are unable to fully address the uncertaity and imperfection of these signals, and then propose the control-physics interactive state-space model and the CPDSE dual estimation framework.

### A. An IBR Example: How Should We Express the State Space?

The structure of a Voltage Source Converter (VSC) with MPPT control is shown in Fig. 1. The physical subsystem includes a DC link, an AC filter, and a source (wind turbines, solar PV panels, or battery arrays). The control subsystem perform digital computation and generate control signals to operate power electronic devices. Although the MPPT control is shown here, it could be substituted by a wide variety of control strategies. The control subsystem influences the state of the physical subsystem by sending control signals, which are transformed into PWM waveforms, to control the on-off switching of the power bridge. Meanwhile, sensors observe output of the physical

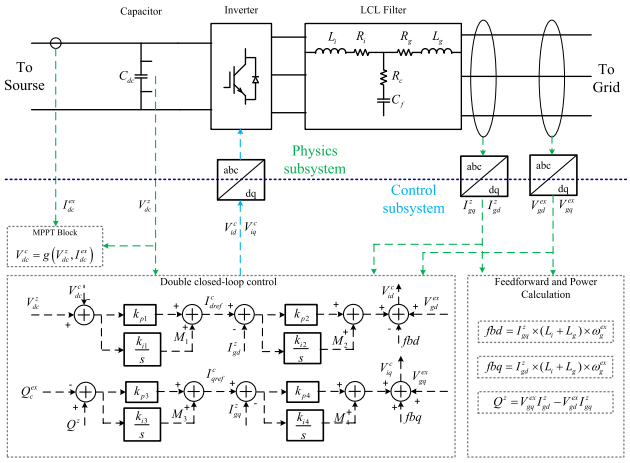


Fig. 1. Structure diagram of GFL based on MPPT control.

subsystem, and feed measurement signals back to determine the state of the control subsystem.

Taking the specific IBR shown in Fig. 1 as an illustrative example, we will discuss the limitations of the traditional blended state-space representation for DSE applications, and introduce the proposed physics-control state-space representation with measurement and control signal interactions.

For the IBR system in Fig. 1, one can write the traditional state-space model widely used by existing DSE methods, in contrast to the proposed state-space model reflecting the reality, as shown in Fig. 2. To avoid distraction from the main philosophy to be discussed, the following simplifications are made in this illustrative example: $V_{dc}^{ex}$ is used as an external input signal; the Phase-Locked Loop (PLL) providing $\omega_g^{ex}$ is not modeled in detail; the model of the power source is not included. However, these factors can be fully considered in the actual implementation of the framework.

As shown in Fig. 1, the physical subsystem influences the control subsystem through the measurement signals $I_{gd}^z$, $I_{gq}^z$, and $V_{dc}^z$. the control subsystem influences the physical subsystem through control signals $V_{id}^c$ and $V_{iq}^c$. These signals are not perfect: noise or even abnormal gross errors may occur due to sensing/actuation imperfection, signal losses and drafts, or even cyber attacks. That is why an random error term $v$ is added to the end of each output equation shown in Fig. 2. *However, the traditional blended state-space representation, as shown on the left of Fig. 2, cannot account for the effect of these signal uncertainties in the state transition equations: the derivative of each state are expressed as a function of other states only.* Specific examples are as follows.

1) *State Transition Equations of the Control Subsystem:* In reality, the transition of the control states ($M_1$, $M_2$, $M_3$, and $M_4$, shown in red) are influenced by measurement signals ($V_{dc}^z$, $I_{gd}^z$, and $I_{gq}^z$, shown in green), as correctly reflected in the proposed control-physics state-space model. However, in the traditional blended state-space model, the state transition equations of the control states (red) must be expressed in terms of the true values of the physical states ($V_{dc}$, $I_{gd}$, $I_{gq}$, etc. as shown in blue), as the control states and the physical states belong to the same state space and the intermediate measurement signals interfacing them should not appear in the state transition equations. This treatment implies that the true values of the physical states (blue) influence the transition of the control states (red) directly, not via the intermediate measurement signals (green) where noise and anomalies may be introduced, which is unrealistic.
2) *State Transition Equations of the Physical Subsystem:* In the same vein, the transition of the physical states ($V_{dc}$, $I_{id}$, $I_{iq}$, etc., shown in blue) are influenced by control signals ($V_{iq}^c$ and $V_{id}^c$, shown in green), as correctly reflected in the proposed control-physics state-space model. However, in the traditional blended state space model, the state transition equations of the physical states (blue) must be expressed in terms of the true values of the control states ($M_1$, $M_2$, $M_3$, and $M_4$, shown in red). This treatment implies that the true values of the control states (red) influence the transition of the physical states (blue) directly, not via the intermediate control signals (green) where noise and anomalies may be introduced, which is unrealistic.

As one of the main functions of DSE is to characterize and combat signal uncertainties, the ignorance of the effects of measurement and control signal imperfections on state transition processes could lead to profound limitations. It prevents the DSE from achieving optimal filtering performance, and may even diverge the DSE when the signal errors are significantly large. It may also prevent the differentiation between the events in the control subsystem and the physical subsystem, as all state variables are blended in the same set of equations. The limitations of the blended state-space representation will be evidently demonstrated via concrete case study results in Section IV.

Different from almost all existing works on DSE for IBRs using the traditional blended state-space model, the proposed CPDSE framework proposed will adopt a control-physics interactive state-space representation. As shown in the right of Fig. 2, it splits the IBR model into two interactive state spaces: the physical state space and the control state space, corresponding to the physical and control subsystems, respectively. Each state space is bounded by the measurement signals and control signals transmitted between subsystems. As such, the transition of a state is only directly influenced by the states of the same subsystem as well as the signals coming from the other subsystem, not by the state of the other subsystem. This is an exact reflection of the situation in an actual IBR system. As such, DSE methods can be designed to fully characterize and combat the uncertainties (possible errors) in these interactive signals.

### B. Control-Physics Interactive State Space Model for IBRs

Generalizing the principles drawn from the specific example in Section II-A, the proposed control-physics state-space representation can be formulated for IBRs as shown in Fig. 3.

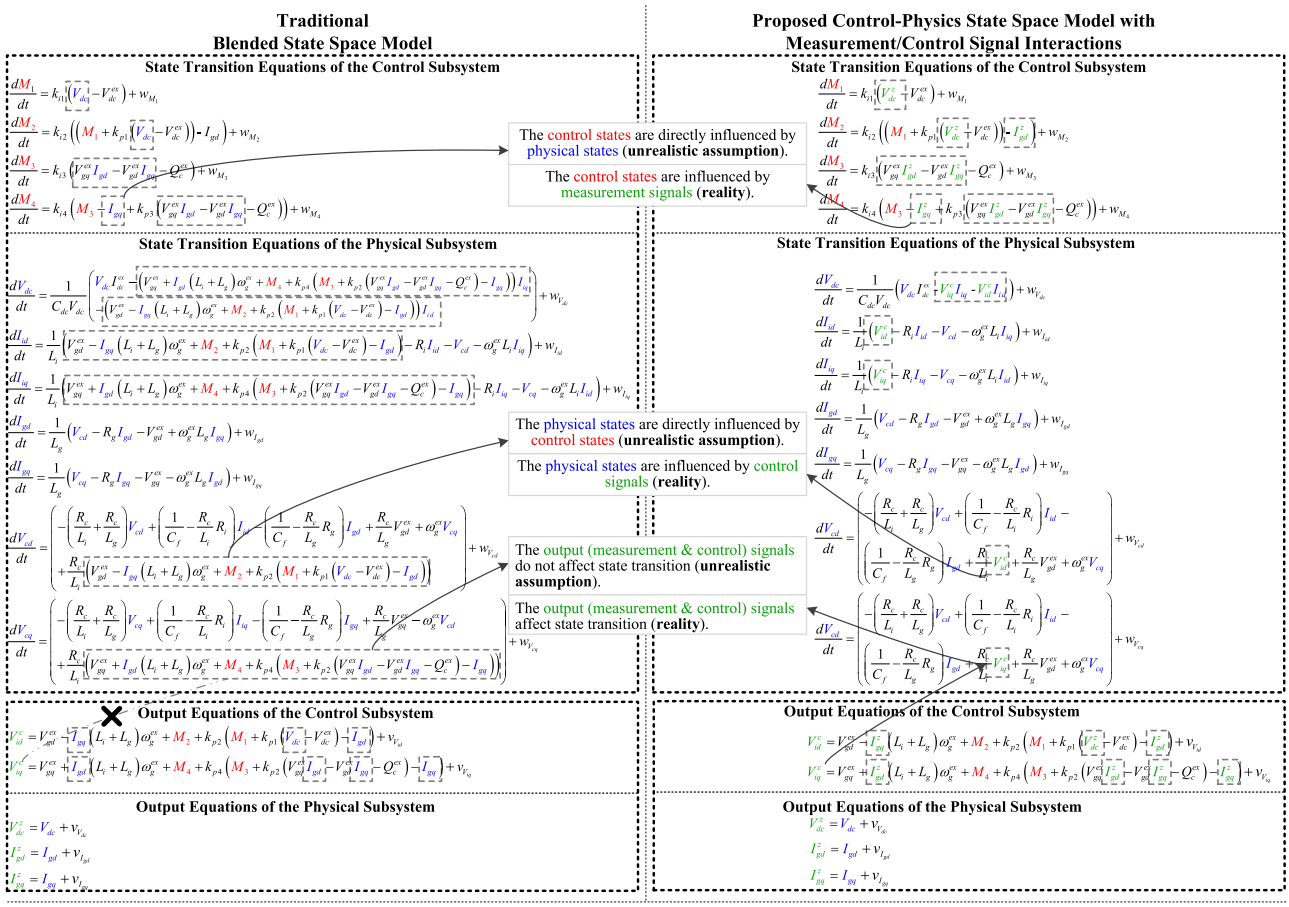


Fig. 2. Representation of an example MPPT-controlled VSC: traditional blended state space versus proposed control-physics interactive state space.

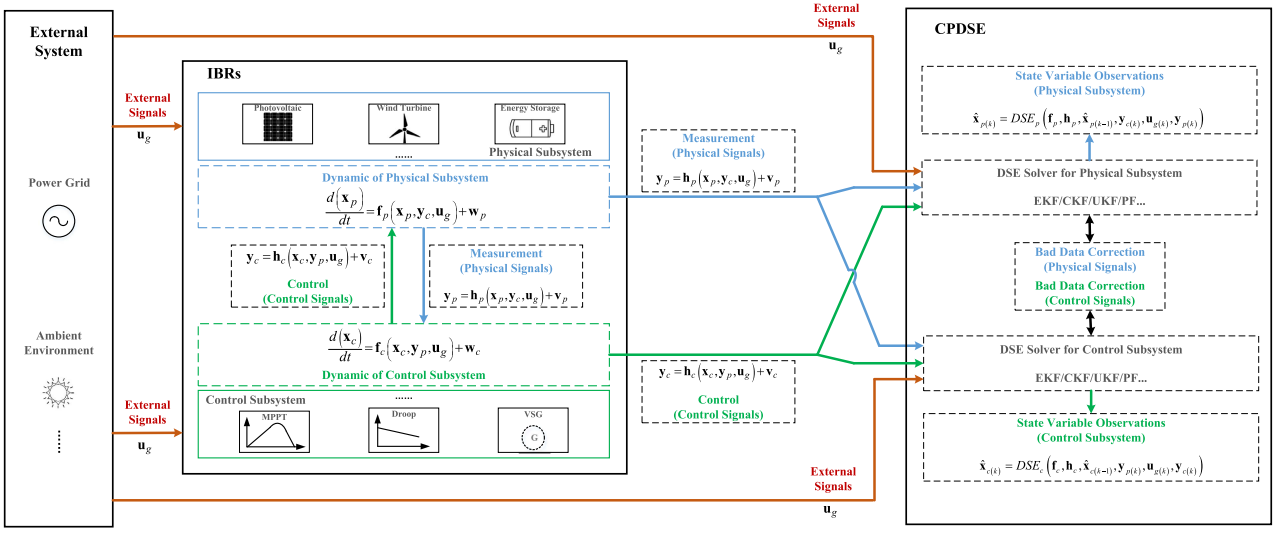


Fig. 3. Generic control-physical state-space representation of IBRs and the proposed CPDSE paradigm.

The state transition equations of the physical subsystem can be represented as follows:

$$\frac{d\mathbf{x}_p}{dt} = \mathbf{f}_p\left(\mathbf{x}_p, \mathbf{y}_c, \mathbf{u}_g\right) + \mathbf{w}_p, \tag{1}$$

where $\mathbf{x}_p \in \mathbb{R}^{n_p \times 1}$ is the state variables of the physical subsystem; $\mathbf{y}_c \in \mathbb{R}^{m_c \times 1}$ is the control signals from the control subsystem; $\mathbf{u}_g \in \mathbb{R}^{l \times 1}$ is the external input signals such as active/reactive power references, ambient conditions, etc.; $\mathbf{w}_p \in \mathbb{R}^{n_p \times 1}$ is the process noise of the physical subsystem due to modeling errors, harmonics, phase imbalance, etc. Taking the MPPT-controlled VSC example shown in Fig. 2, $\mathbf{x}_p$ refers to the physical state variables in blue, e.g., $V_{dc}$, $I_{gd}$, $I_{gq}$, etc., and $\mathbf{y}_c$ refers to the outputs of the control subsystem in green, i.e., $V_{id}^c$ and $V_{iq}^c$.

Measurement signals are the outputs of the physical subsystem. The output equations of the physical subsystem are:

$$\mathbf{y}_p = \mathbf{h}_p\left(\mathbf{x}_p, \mathbf{y}_c, \mathbf{u}_g\right) + \mathbf{v}_p, \tag{2}$$

where $\mathbf{y}_p \in \mathbb{R}^{m_P \times 1}$ is the output variables of the physical subsystem, i.e., measurement signals; $\mathbf{v}_p \in \mathbb{R}^{m_P \times 1}$ is the output noise due to sensing noise, drifts or failures. Similarly, in the example shown in Fig. 2, $\mathbf{y}_p$ represents the measurement signals in green, i.e., $V_{dc}^z$, $I_{gd}^z$, and $I_{gq}^z$.

The state transition equations of the control subsystem can be represented as follows:

$$\frac{d\mathbf{x}_c}{dt} = \mathbf{f}_c\left(\mathbf{x}_c, \mathbf{y}_p, \mathbf{u}_g\right) + \mathbf{w}_c, \tag{3}$$

where $\mathbf{x}_c \in \mathbb{R}^{n_c \times 1}$ is the state variables of the control subsystem, e.g., $M_1$, $M_2$, $M_3$, and $M_4$ in the example shown in Fig. 2; $\mathbf{w}_c \in \mathbb{R}^{n_c \times 1}$ is the process noise of the control subsystem representing the uncertainty of state transition due to discretization, computation error, cyber attacks, etc.

Control signals are the outputs of the control subsystem. The output equations of the control subsystem are given by:

$$\mathbf{y}_c = \mathbf{h}_c\left(\mathbf{x}_c, \mathbf{y}_p, \mathbf{u}_g\right) + \mathbf{v}_c, \tag{4}$$

where $\mathbf{v}_c \in \mathbb{R}^{m_c \times 1}$ is the output noise representing the uncertainty of control signals due to latency, actuation imperfection, or cyber attacks.

### C. Dual CPDSE Solvers

From the power grid operators' point of view, the internal states of the digital controllers, which play important roles in IBR dynamics, cannot be directly observed since manufacturers are unlikely to provide interfaces to output them. For example, for IBRs with VSG control, the virtual "rotor speed" and "power angle" are critical information for grid operators yet are often unreported. Therefore, the *objective* of DSE for IBRs is to track the state variables of both the physical subsystem and the control subsystem of the IBRs in the presence of noise and even bad data in the outputs of each subsystem, i.e., in measurement signals and control signals.

From Equations (1)–(4) and Fig. 3, an interesting fact can be observed: *there is a structural symmetry between the physical subsystem and the control subsystem.* The outputs of the physical subsystem, which are the measurement signals, are the inputs of the control subsystems. The outputs of the control subsystem, which are the control signals, are the inputs of the physical subsystem. Therefore, we propose to use two dual estimators – a Physical Dynamic State Estimator (PDSE) and a Control Dynamic State Estimator (CDSE) – to track IBR states. At time step $k$, the generic form of the proposed CPDSE framework can be generally expressed as follows.

$$\widehat{\mathbf{x}}_{p(k)} = DSE_p\left(\mathbf{f}_p, \mathbf{h}_p, \widehat{\mathbf{x}}_{p(k-1)}, \mathbf{y}_{c(k)}, \mathbf{u}_{g(k)}, \mathbf{y}_{p(k)}\right), \tag{5}$$

$$\widehat{\mathbf{x}}_{c(k)} = DSE_c\left(\mathbf{f}_c, \mathbf{h}_c, \widehat{\mathbf{x}}_{c(k-1)}, \mathbf{y}_{p(k)}, \mathbf{u}_{g(k)}, \mathbf{y}_{c(k)}\right), \tag{6}$$

where $DSE_p$ and $DSE_c$ represent dynamic state estimators for the physical subsystem and the control subsystem, respectively. They could be realized by a variety of methods, such as EKF, UKF, CKF, or others. As illustrated in Fig. 3, the PDSE in (5) aims to obtain the estimates of the physical subsystem state variables, $\widehat{\mathbf{x}}_{p(k)}$. It requires its state transition function $\mathbf{f}_p$, output function $\mathbf{h}_p$; external signals $\mathbf{u}_{g(k)}$, state estimate of the previous step $\widehat{\mathbf{x}}_{p(k-1)}$, output of the physical subsystem $\mathbf{y}_{p(k)}$, and output of the control subsystem $\mathbf{y}_{c(k)}$. Thanks to the elegant *duality* nature of the system, the CDSE in (6) has a symmetrical structure, where variables in one subsystem are replaced by their counterparts in the other subsystem, except for external signals $\mathbf{u}_{g(k)}$ required by both subsystems.

It requires special attention that although the outputs of both subsystems, $\mathbf{y}_{p(k)}$ and $\mathbf{y}_{c(k)}$, are taken by both PDSE and CDSE, they have opposite roles in the two estimators. In PDSE, measurement signals $\mathbf{y}_{p(k)}$ are the outputs of the subsystem, and control signals $\mathbf{y}_{c(k)}$ are inputs of the subsystem. On the contrary, in CDSE, control signals $\mathbf{y}_{p(k)}$ are the outputs, and measurement signals $\mathbf{y}_{c(k)}$ are the inputs. Each estimator checks the consistency between the model and the output signals of the corresponding subsystem, hence PDSE and CDSE can filter noise and detect bad data in measurement signals and control signals, respectively.

The proposed CPDSE framework is generic and applicable to arbitrary types of IBRs with various power sources, power electronic converters, and control algorithms. It also allows various choices of DSE algorithms for both PDSE and CDSE. In this paper, we will materialize the CPDSE framework with an ACKF algorithm with bad data processing functions. The details of the algorithm will be introduced in Section III.

## III. Adaptive Cubature Kalman Filter for DSE and Bad Data Processing

This section will present a detailed algorithm for materializing the generic CPDSE framework proposed in Section II.

### A. ACKF-Based Dual CPDSE Algorithm

As IBRs are typically nonlinear systems, CKF, which propagates system uncertainties with high accuracy and computational efficiency, is a good option as the DSE solver. However, for power electronic systems, the statistics of the process noise and output noise are typically unknown, which makes the setting of noise covariance matrix challenging and often sub-optimal.

Therefore this paper will devise an ACKF to estimate the noise statistics simultaneously with the state variables in real time. We will also embed bad data detection function to further enhance its robustness.

With the *duality* of the two subsystems, the ACKF-based CDSE and PDSE algorithms can be described uniformly. Denote a subscript index set $\Omega = \{p, c\}$, where "$p$" represents variables associated with the physical subsystem, and "$c$" represents those associated with the control subsystem. Suppose $\phi \in \Omega$, and $\bar{\phi}$ is the complement of $\phi$ on $\Omega$. The discretized state transition equations and output equations of a subsystem $\phi \in \Omega$ can be expressed as follows:

$$\mathbf{x}_{\phi(k)} = \mathbf{f}_\phi\left(\mathbf{x}_{\phi(k-1)}, \mathbf{y}_{\bar{\phi}(k-1)}, \mathbf{u}_{g(k-1)}\right) + \mathbf{w}_{\phi(k)}, \quad (7)$$

$$\mathbf{y}_{\phi(k)} = \mathbf{h}_\phi\left(\mathbf{x}_{\phi(k)}, \mathbf{y}_{\bar{\phi}(k)}, \mathbf{u}_{g(k)}\right) + \mathbf{v}_{\phi(k)}, \quad (8)$$

where $\mathbf{w}_{\phi(k)} = N(\mathbf{0},\ \mathbf{Q}_{\phi(k)})$ and $\mathbf{v}_{\phi(k)} = N(\mathbf{0},\ \mathbf{R}_{\phi(k)})$. For a state space, $\mathbf{x}_{\phi(k)} \in \mathbb{R}^{n_\phi \times 1}$, the ACKF algorithm uses the third-order spherical radial rule to generate a set of $2n_\phi$ cubature points, and weights them equally to approximate the probability distribution propagating through a nonlinear function. The cubature points are selected as follows:

$$w_{\phi i} = \frac{1}{2n_\phi}, \quad i = 1, 2, \ldots 2n_\phi, \quad (9)$$

$$\Xi_\phi = \xi_{\phi i, i=1..2n} = \sqrt{n_\phi}\,(I_n, -I_n), \quad (10)$$

where $I_n$ represents an $n$-dimensional identity matrix. After initialization, the CPDSE algorithm can be executed with the flowchart shown in Fig. 4. Steps 1 to 3 are the steps of the conventional CKF, which include state prediction, output prediction, Kalman gain computation [26], [27], [28]. Step 4 describes the bad data detection approach. It is accomplished by the Largest Normalized Residual (LNR) test [29]. Normalized residuals can be evaluated as:

$$\mathbf{r}_k = (\mathbf{P}_{yy,k+})^{-\frac{1}{2}}\left(\mathbf{y}_{\phi(k)} - \mathbf{h}_\phi\left(\widehat{\mathbf{x}}_{\phi(k)}, \mathbf{y}_{\bar{\phi}(k)}, \mathbf{u}_{g(k)}\right)\right). \quad (11)$$

where $\mathbf{P}_{yy,k+}$ is the auto-covariance matrices of the predicted outputs at time $k$ computed in Step 4. The LNR is found as:

$$u = \arg\max_j \left\{\mathbf{r}_k^j, j = 1, 2 \ldots, m_\phi\right\}. \quad (12)$$

If the absolute value of LNR is greater than a set threshold, i.e., $|\mathbf{r}_k^u| > t$, the $u$-th measurement is identified as a bad data. Assuming Gaussian distribution, $t$ is typically set as 3.0, corresponding to 99.74% confidence level. Then, Step 5 performs bad data correction by replacing the identified bad data $\mathbf{y}_{\phi(k)}^u$ as follows:

$$\mathbf{y}_{\phi(k)}^u - \frac{\mathbf{R}_{\phi(k)}^{uu}}{\mathbf{P}_{yy,k+}^{uu}}\left(\mathbf{y}_{\phi(k)} - \mathbf{h}_\phi\left(\widehat{\mathbf{x}}_{\phi(k)}, \mathbf{y}_{\bar{\phi}(k)}, \mathbf{u}_{g(k)}\right)\right). \quad (13)$$

After correction, the algorithm will return to Step 3 and repeat. For applications which only record abnormal events without the need for bad data correction, Step 5 can be skipped.

The last step of ACKF, i.e., Step 6, updates the noise covariance matrices $\mathbf{Q}_{\phi(k)}$ and $\mathbf{R}_{\phi(k)}$. Adaptive KF can be divided into four broad categories: covariance matching, Bayesian, correlation-based, and maximum likelihood [30]. This paper employs the innovation-based adaptive estimation method [31].

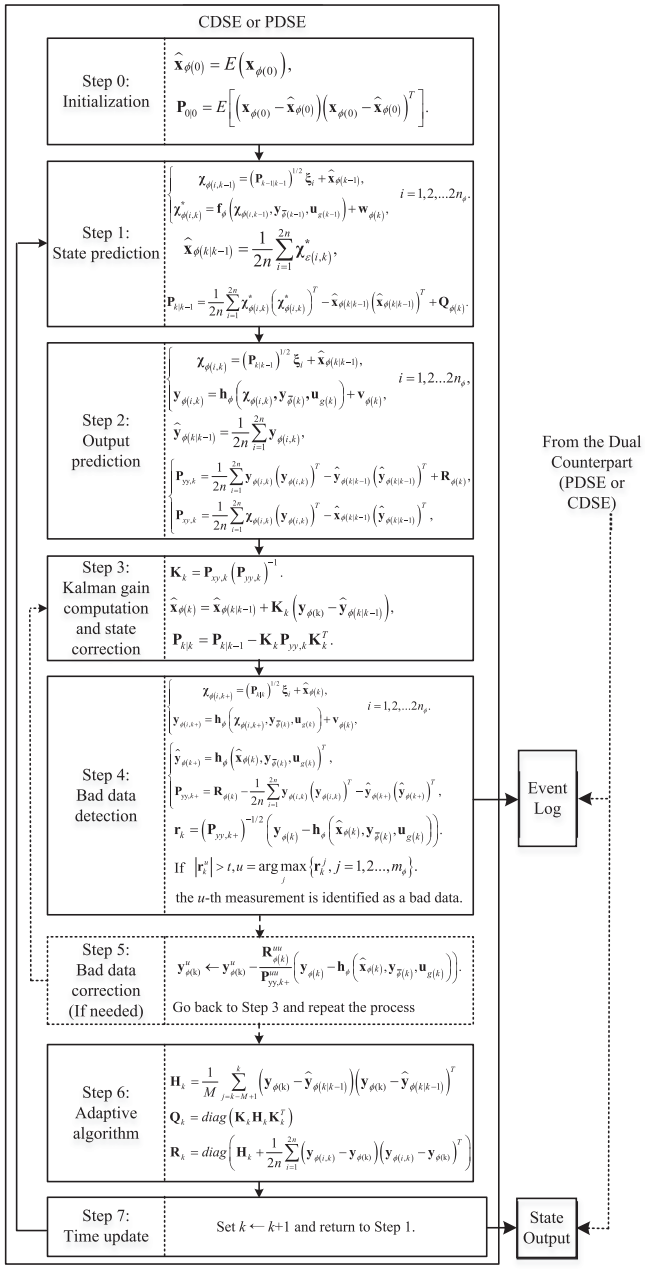


Fig. 4. Proposed ACKF-based dual CPDSE algorithm.

For PDSE and CDSE, the ACKF-based DSE solver is adopted with different values of $\phi \in \Omega = \{c,\ p\}$. Each estimator needs to use the models, state variables, and output variables of the corresponding subsystem ($\mathbf{f}_\phi, \mathbf{h}_\phi, \widehat{\mathbf{x}}_\phi, \widehat{\mathbf{y}}_\phi$), and the output variables of the other subsystem ($\widehat{\mathbf{y}}_{\bar{\phi}}$) serve as inputs. When both subsystems have completed the DSE at time $k$, they move to the next time step.

The LNR-based bad data detection of each estimator checks the consistency between the model and the output signals of the corresponding subsystem. Therefore, *PDSE will detect and correct bad data in measurement signals, and CDSE will detect and correct bad data in control signals*. Thanks to the explicitly

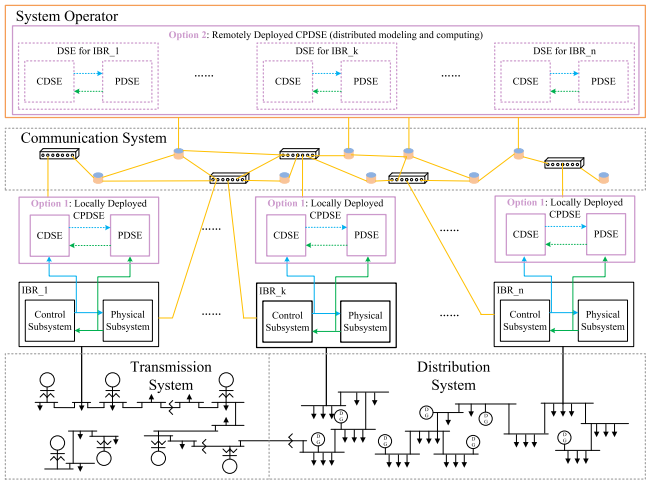


Fig. 5. Two potential implementation paradigms for the proposed technique.

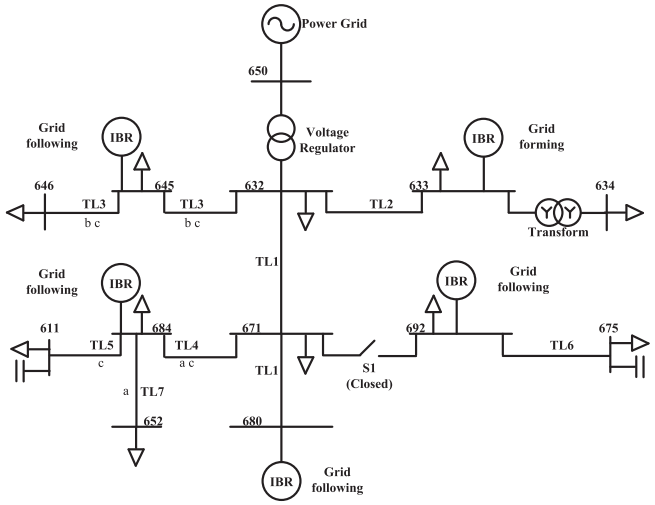


Fig. 6. One-line diagram of IEEE 13-node test feeder with 5 IBRs.

modeled interacting signals between the two subsystems, the true source of bad data can be located among all the measurement signals and control signals.

This paper devises the ACKF algorithm as the DSE solver in CPDSE framework, considering its good tradeoff between accuracy and computational efficiency. However, other DSE algorithms, such as the more expensive EnKF and PF, can replace ACKF as the DSE solver in the CPDSE framework as well, as long as the computational power satisfies the requirements under the relatively small time steps compared with DSE for SGs.

### B. Implementation Paradigm

The CPDSE framework is purposed to be implemented distributedly for each IBR in a power system. This means that the state-space model should be established for each IBR (not the entire power grid), and the resulting DSE algorithm should estimate the corresponding states of the IBR. All external signals from other IBRs or the control center are taken as input variables. Since the order of the model of a single IBR is limited, the fully distributed CPDSE algorithm does not have scalability issues even in large-scale power systems.

In practice, there are two potential paradigms for implementing the proposed CPDSE framework, as shown in Fig. 5. The first option is to implement the CPDSE locally on each IBR's site, where the impact of communication delays can be neglected. The second option is to implement the CPDSE remotely at system operators' control center, in which case the measurement signals and control signals required should be transmitted using communication protocols such as IEC 61850, and timestamps are required for aligning the data points. There has been much existing effort on synchronized waveform measurements that can satisfy the time synchronization requirements for carrying out the CPDSE remotely [23], [32]. It should be noted that even when the remote CPDSE option is implemented, the algorithm still maintains a fully distributed manner for each individual IBR. Therefore, distributed computing can readily be applied to fully utilize the computational resources at a control center.

## IV. Simulation Results

This section will verify the advantages and versatility of the proposed concept and algorithm in multipel test systems full EMT simulation. Firstly, CPDSE will be carried out on two PV systems in the IEEE 13-node test feeder with different (grid-following and grid-forming) control methods. A comparative study will be presented to show the superiority of the proposed CPDSE framework over the traditional method based on blended state-space models. Then, the versatility of the CPDSE framework will be demonstrated on a grid-following-controlled PMSG-WT connected to the IEEE 34-node test feeder hosting various types of IBRs and dynamic loads. Finally, the effectiveness of CPDSE in the transmission system will be validated with a BESS operating in the VSG mode with a rated power of 20 MW in the IEEE 10-machine 39-bus test system.

The true state of the system is simulated via Simulink (Version 10.5, R2022a), and the CPDSE algorithms are implemented in MATLAB (Version 9.12, R2022a). The data sampling frequency is set as 3840 Hz (64 points per cycle), which is readily satisfied by state-of-the-art merging units (MUs), digital fault recorders (DFRs), or smart inverters. Note that MUs and DFRs have been widely considered for DSE in literature [23], and smart inverters also have the capability of outputting data for DSE as per the new IEEE standard [32].

### A. Case 1: Comparison With Traditional DSE Using Blended State Space Model in the IEEE 13-Node Test Feeder

In this case, 5 IBRs, i.e., PV generation systems of various types, are integrated into the system shown in Fig. 6. They include one three-phase IBR in the VSG (grid-forming) control mode (node 633), two three-phase IBRs in the MPPT (grid-following) control mode (nodes 692 and 680), and two single-phase IBRs in the MPPT (grid-following) control mode (nodes 645 and node 684). The parameters of the system are shown in Table I. The rated capacities of the three-phase IBRs and single-phase IBRs are 500 MVA and 80 MVA, respectively. The one-line diagram of the system is shown in Fig. 6. Here, we

TABLE I
PARAMETERS OF IBRS IN CASE 1

| Physical Subsystem | | Control Subsystem of GFL | | Control Subsystem of GFM | |
|---|---|---|---|---|---|
| $L_i$ | 4.2mH | $K_{p1}$ | 1.5 | $J$ | 5 |
| $R_i$ | 10mΩ | $K_{i1}$ | 60 | $D_p$ | 120 |
| $L_g$ | 1.3mH | $K_{p2}$ | 0.2 | $K_q$ | 0.6 |
| $R_g$ | 10mΩ | $K_{i2}$ | 40 | $D_q$ | 12 |
| $C_f$ | 30uF | $K_{p3}$ | 0.8 | $K_{qp}$ | 25 |
| $R_f$ | 0.5Ω | $K_{i3}$ | 40 | $T_d$ | 1 |
| $C_{dc}$ | 5mF | $K_{p4}$ | 0.2 | $K_{qp}$ | 0.6 |
| | | $K_{i4}$ | 40 | $K_{qi}$ | 60 |

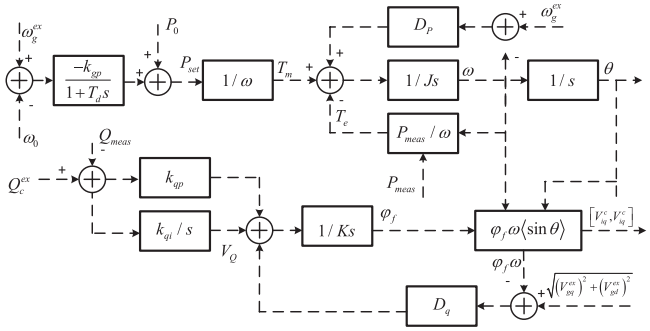


Fig. 7. Grid-forming control example: VSG control.

consider each solar PV system to have only one power bridge, i.e., the grid-interfaced inverter. Therefore, regardless of the control mode, the control signals are always $V_{id}^c$ and $V_{id}^c$, the reference voltage of power bridge; the measurement signals are $I_{gd}^z$ and $I_{gd}^z$, the grid side current of LCL filter, and $V_{DC}^z$, the voltage of DC-side capacitor.

The structure and control block diagram of the MPPT-controlled three-phase IBRs are shown in Fig. 1. The physical subsystem of the IBR in the VSG mode is the same as the one in the MPPT node; only the control subsystem is differently designed as shown in Fig. 7. For CPDSE, it is only necessary to replace the state transition equation of CDSE, and the PDSE model remains the same.

Initially, the IBR with MPPT control at node 692 operates with an active power output of 0.92 p.u. and a reactive power output of 0 p.u.; a step change of reactive power reference from 0 p.u. to 0.25 p.u. and a step change of solar irradiance from 0.92 p.u. to 0.52 p.u. are introduced at at 1.5 s and 2.5 s, respectively. For GFM at node 633, a -0.6 Hz step change of the system frequency is introduced at 3.5 s.

*1) Comparison of Traditional and Proposed Methods During Normal Operation:* To represent sensor imperfection, Gaussian white noises with standard deviations of 1% and 0.5% are added to the current measurement signals and the DC voltage measurement signals, respectively. For the control signals, imperfection naturally exist when they are transformed through the SVPWM method, so no additional noise needs to be added.

To demonstrate the superiority of the CPDSE framework, which is based on the control-physics interactive state-space model, it is compared with the traditional method that relies on the blended state-space model. Both methods applies the same ACKF technique; the information redundancy is also the same, as the same sets of signals are used for performing DSE (see

TABLE II
RMSES OF STATE ESTIMATES OF IBRS WITH MPPT AND VSG CONTROLS

| States | Blended | Proposed | States | Blended | Proposed |
|---|---|---|---|---|---|
| $V_{DC}$ | 0.16% | 0.16% | $V_{DC}$ | 0.08% | 0.08% |
| $I_{id}$ | 0.78% | 0.82% | $I_{id}$ | 0.78% | 0.80% |
| $I_{iq}$ | 0.73% | 0.80% | $I_{iq}$ | 0.69% | 0.73% |
| $I_{gd}$ | 0.69% | 0.67% | $I_{gd}$ | 0.53% | 0.56% |
| $I_{gq}$ | 0.68% | 0.66% | $I_{gq}$ | 0.52% | 0.57% |
| $V_{cd}$ | 1.33% | 1.14% | $V_{cd}$ | 0.74% | 0.76% |
| $V_{cq}$ | 1.29% | 1.08% | $V_{cq}$ | 0.61% | 0.62% |
| $M_1$ | 0.10% | 0.08% | $P_{set}$ | 0.10% | 0.10% |
| $M_2$ | 0.12% | 0.11% | $\omega_i$ | **3.88%** | **0.39%** |
| $M_3$ | 0.07% | 0.08% | $\Delta_\theta$ | 1.03% | 0.10% |
| $M_4$ | 0.10% | 0.10% | $V_Q$ | **2.94%** | **0.31%** |
| | | | $\phi_f$ | 0.04% | 0.005% |

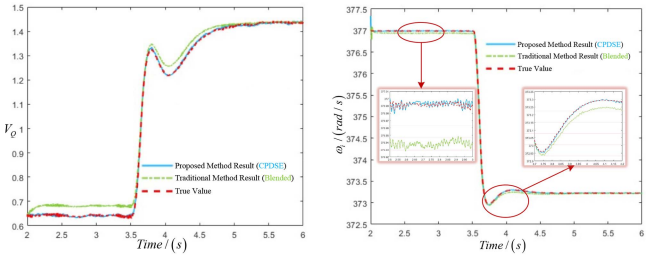


(a) $V_Q$ (b) $\omega_i$

Fig. 8. True and estimated states under normal operation of VSG control.

output variables in Fig. 2). The system is observable as the output signals are related to all the state variables.

The performances of the traditional and proposed methods are compared by the Root Mean Square Error (RMSE) of state variables, as shown in Table II. It can be observed that for both methods, the errors of state estimates are in a reasonable range, demonstrating the effectiveness of the ACKF technique for tracking the states under normal operating conditions. For the IBR under the MPPT control, the difference between the two methods is not very significant. However, for the IBR under VSG control, it is found that significant estimation errors are present for some control state variables, i.e., $\omega_i$ and $V_Q$, when using the traditional blended state-space representation. The true trajectory and estimated trajectories by the two methods are shown in Fig. 8. It can be found that the estimated trajectory by the traditional method significantly deviates from the true trajectory, while the one by the proposed method almost overlaps with the true one. The reason is that these two state variables are highly sensitive to the imperfection of output signals. As the traditional blended state-space model does not have the capability to represent these imperfections, The DSE fails to filter them properly, leading to large state estimation errors. Note that $\omega_i$ is the virtual "rotor speed" of the VSG, which is a critical variable to track. The proposed CPDSE framework is evidently advantageous for this task.

*2) Comparison of DSE Results During Abnormal Operation:* For IBRs, abnormality can be present in either measurement signals or control signals for reasons explained in Section II-B. The traditional method uses the blended state-space model without the capability of accounting for the impacts of abnormalities in

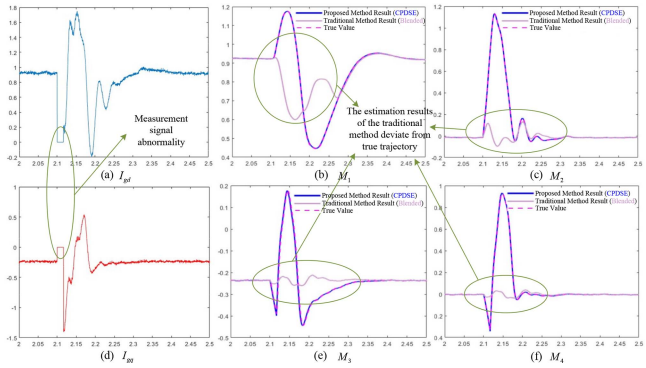


Fig. 9. True and estimated states of grid-following IBR (MPPT control) under measurement signal abnormalities.

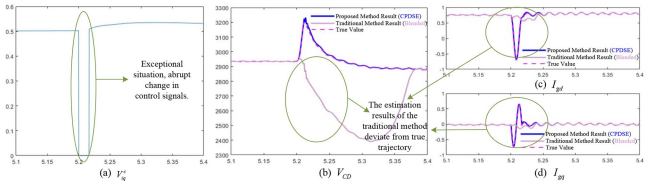


Fig. 10. True and estimated states of grid-forming IBR (VSG control) under control signal abnormalities.

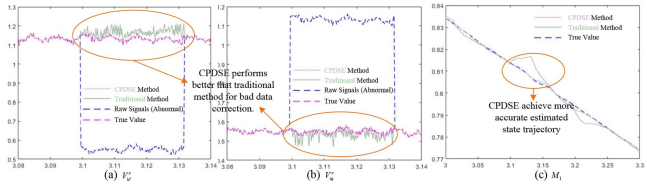


Fig. 11. Bad data correction for grid-following IBR (MPPT control) under control signal abnormalities.

these signals between the two subsystems, as they do not appear in the state transition equations.

We first use an example of measurement abnormality, which commonly exists in the real world, to illustrate the issue. An IBR measures the grid current with a current sensor and transmits the signal to the IBR's controller through copper wire or optical fiber. Assuming that at 2.1 s, the IBR in the MPPT control mode has an unreliable cable connection, causing grid current measurements $I_{gd}^z$ and $I_{gq}^z$ to be zero within one cycle before returning to normal. During this period, the IBR continues to operate. In this case, it is assumed that the objective of DSE is to objectively track the actual transient occurring in the IBR due to the abnormal measurement signals, and thus bad data detection and correction functions are not activated. The verification of bad data processing functions will be left to a scenario presented later.

The true trajectories and the estimated trajectories of the control states $M_1$ - $M_4$ by the traditional and proposed methods are shown in Fig. 9. It is observed that the erroneous measurements affect the states of the control subsystem, as they are the inputs of the control subsystem. While the result of the proposed CPDSE keeps close track of the true trajectory of the control subsystem, the result of traditional DSE method based on the blended state-space model drastically deviates from the true trajectory. The reason of divergence is exactly what has been theoretically analyzed in Section II: in the traditional blended state-space representation, measurement signals do not appear in the state transition equations, and thus the errors of these signals cannot find their paths to affect state predictions in DSE, and therefore the state trajectory estimated by DSE is completely wrong.

Similarly, we present another case where the control signals $V_{id}^c$ and $V_{iq}^c$ drop to zero at 5.2 s due to cyber attacks or fiber optic abnormalities, etc. Fig. 10 shows the true and estimated trajectories of the physical states. As control signals are the inputs of the physical subsystem, the physical states are severely disturbed as expected. The proposed method tracks the true state trajectory very well, while the traditional method has large estimation errors during the transient.

*3) Bad Data Detection and Correction:* In the scenario presented above, the bad data detection and correction functions of the DSEs are turned off such that the actual transients within the IBR system are objectively observed. In this scenario, the bad data functions are activated to recover the correct signals should the abnormality be absent.

Due to the limited space, we only show the results of a simulation where abnormality occurs in the IBR in the grid-following MPPT control mode. It is assumed that the control signals in two channels, $V_{cd}$ and $V_{cq}$, are swapped due to electromagnetic interference (e.g., electronic register malfunction) or malicious cyber attacks. The raw signals and corrected signals by the traditional and proposed methods are shown in Fig. 11(a), (b). It is found that both methods provide capabilities to recover the signals to certain extents: the corrected ones are closer to the true values than the raw control signals. However, the proposed CPDSE framework recovers the signals much more accurately than the traditional one. Fig. 11(c) shows the true and estimated trajectories of a control state, $M_1$, which is directly estimated from the output control signals. It is evident that the proposed method estimates the state more accurately than the traditional one.

*4) Summary:* Through the various simulation scenarios of Case 1, we have demonstrated the superiority of the CPDSE framework. Under normal operating conditions, the proposed method is evidently advantageous for estimating states that are highly sensitive to noise in measurement and control signals, including critical ones such as the virtual roter speed of VSG control. Under abnormal measurement and control signals, the traditional DSE method diverges drastically from the true state trajectories, while the proposed method manifests robust state tracking and bad data processing performance. The superiority under various conditions is attributed to the fact that the proposed CPDSE framework fully accounts for the uncertainties in measurement and control signals that interact between the physical and control subsystems, which the traditional method ignores.

### B. Case 2: Demonstration of Versatility for Various IBRs

In Case 1, simulation results for solar PV systems under grid-following and grid-forming control modes are presented.

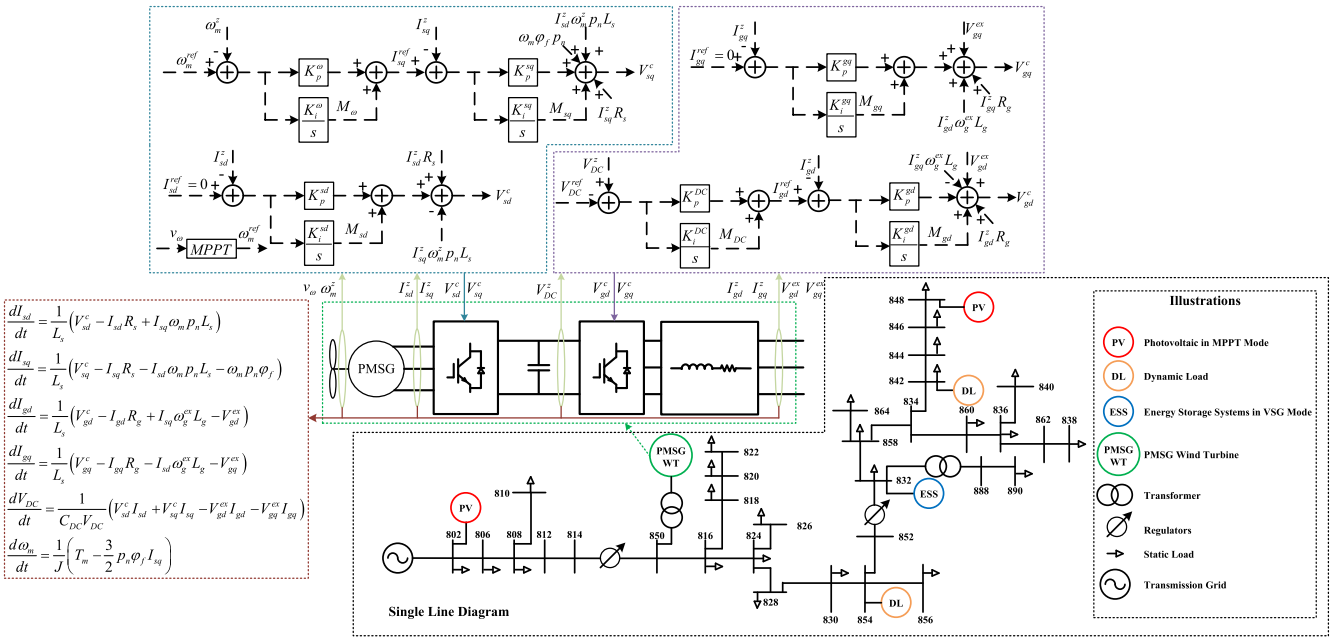


Fig. 12. PMSG control block diagram and related equations in IEEE 34-node test feeder.

In order to demonstrate the versatility of the proposed CPDSE framework, in Case 2, we will present results for a PMSG-WT connected to a more complex IEEE 34-node test feeder. The PMSG-WT operates in the grid-following MPPT control mode. In addition to the PMSG-WT, solar PV systems under MPPT control, BESSs under VSG control, and dynamic loads are also connected to the test feeder. While Case 1 is simulated in a per-unit system, the PMSG-WT is simulated in actual values in Case 2. The system one-line diagram and the PMSG-WT control block diagram are shown in Fig. 12. The electromechanical wind turbine model is included as part of the state-space model [12], [13]. Due to limited space, the derivation of the state transition equations and output equations will not be shown.

In this example, the initial wind speed is 8 m/s, and the output power of the PMSG-WT is 580 kW. From 2 s to 2.5 s, the wind speed increases to 9 m/s, and the output power increases correspondingly to 820 kW. The four control signals $V_{sd}^c$, $V_{sq}^c$, $V_{gd}^c$ and $V_{gq}^c$ are added with noise that follows a Gaussian distribution $N(0, 2.5^2)$. The four current measurement signals $I_{sd}^z$, $I_{sq}^z$, $I_{gd}^z$ and $I_{gq}^z$ are added with noises that follow a Gaussian distribution $N(0, 5^2)$. Noises following Gaussian distributions $N(0, 0.1^2)$ and $N(0, 2^2)$ are added to the PMSG electrical angular velocity ${\omega_m}^z$ and the DC-side capacitor voltage $V_{DC}^z$, respectively. In order to demonstrate the effectiveness of the ACKF, it is assumed that the above noise statistics are unbeknownst to the DSE algorithm initially. The adaptive estimation of noise statistics is activated at 1.5 s.

Despite very different natures of the PMSG-WT from the solar PV system demonstrated in Case 1, the duality of the control-physics interactive state-space model is still valid. The control signals are outputs of the control subsystem and inputs to the physical subsystem, affecting the six physical state variables. The measurement signals are outputs of the physical subsystem and inputs to the control subsystem, influencing the six control state variables, as shown in Fig. 12. Therefore, the CPDSE framework can be applied in the same manner.

The true and estimated trajectories of all the six control states and all the six physical states are shown in Fig. 13. It can be seen that initially when the noise statistics are unknown, the estimation results are unsatisfactory as noise covariance matrices in DSE are random set and do not reflect the true statistics. Starting from 1.5 s, the noise covariance estimation function of the proposed ACKF algorithm is activated, and the estimated values soon converge to the true values. For the rest of the simulation, the algorithm tracks all the physical and control states accurately. The results verify that the noise adaptation feature of ACKF can greatly reduce the estimation error under unknown noise statistics, which is usually encountered in real-world applications to IBRs due to the unknown properties of sensors, actuators, and systems. Besides results shown in Fig. 12, additional simulations are conducted in the presence of measurement and control signal abnormalities, and it is verified that the CPDSE works satisfactorily in bad data processing. The results are not presented due to limited space. Hence, it is validated that the proposed CPDSE framework is applicable to not only PV systems but also wind generators.

### C. Case 3: Demonstration on IBRs in Transmission Systems

Through Case 1 and Case 2, we have validated the effectiveness of the proposed method on different types of IBRs in distribution systems. In Case 3, we will verify that this method remains effective in transmission systems. As the proposed method has been validated on a solar PV system and a PMSG-WT, in Case 3, we will validate it on a BESS operating in the

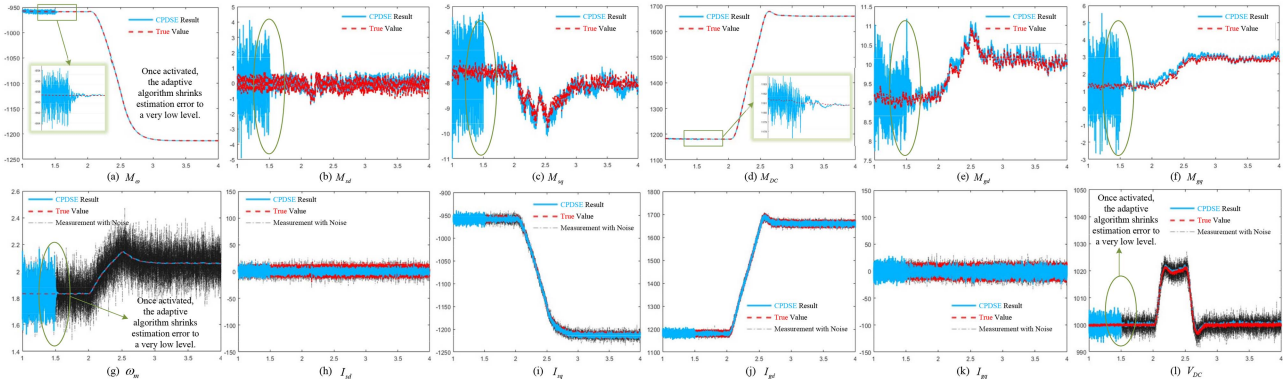


Fig. 13. State estimation results of PMSG-WT based on CPDSE.

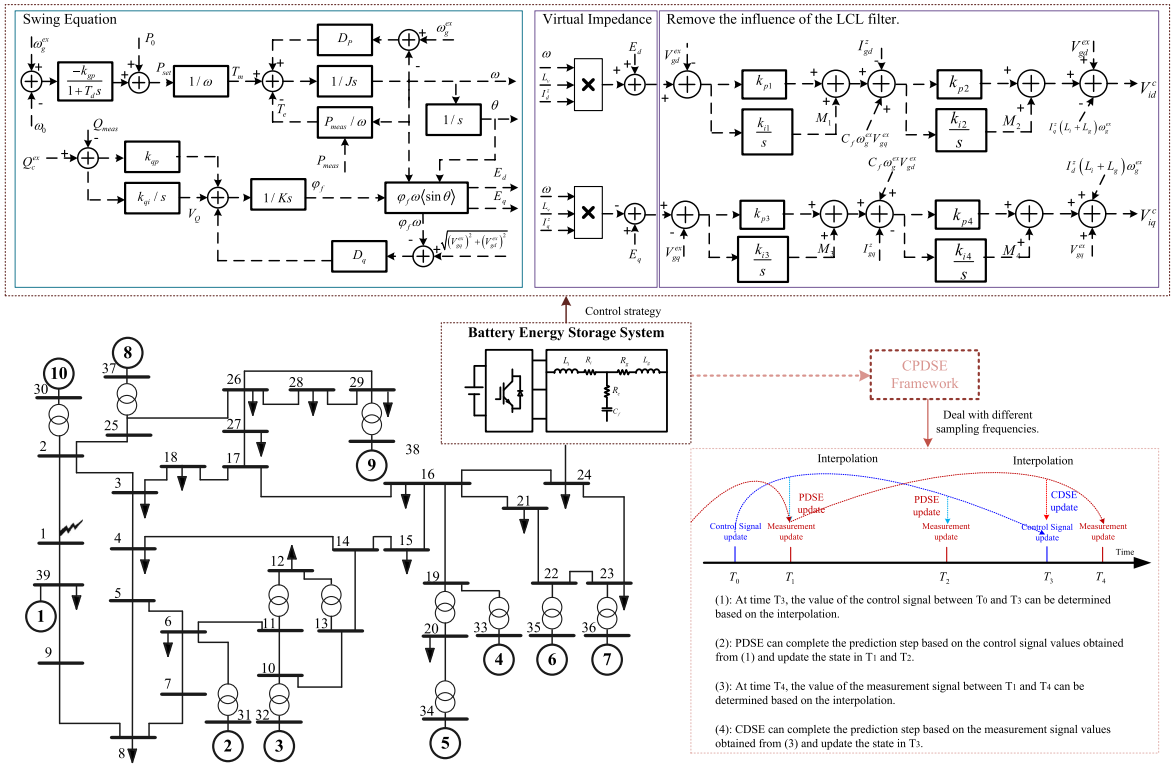


Fig. 14. Battery energy storage system integrated into the IEEE 39-bus system.

VSG mode. The power system one-line diagram and the BESS schematic are shown in Fig. 15.

Considering the possible difference of time resolutions of control and measurement signals in IBRs, in Case 3, we assume a sampling frequency of 3840 Hz for measurements, while control signals are transmitted to the DSE at a frequency of 1920 Hz. In this scenario, the CPDSE handles the different data resolutions using the method shown in Fig. 15, which can be divided into four steps. Step 1: interpolate the control signals between time $T_0$ and $T_3$; Step 2: utilize the control signals obtained in Step 1 and the measurements complete the PDSE at times $T_1$ and $T_2$; Step 3: interpolate the measurement between time $T_1$ and $T_4$; Step 4: utilize the measurements obtained in Step 3 and the control signal complete the CDSE at times $T_3$.

The BESS has a rated capacity of 20 MW. At 15 s, a three-phase short-circuit fault occurs near bus 1, lasting for 4 cycles, simulating the impact of a remote fault on the BESS. The noises in the control signals ($V_{id}^c$ and $V_{iq}^c$, the reference voltage of power bridge) and measurement signals ($I_{gd}^z$ and $I_{gq}^z$, the grid side current of LCL filter) are Gaussian white with standard deviations of 1% and 1.25%, respectively.

The results are shown in Fig. 14. Among them, the voltage and reactive power output after the remote fault and its clearance are plotted in Fig. 14(a). It can be observed that the BESS in the VSG mode provides reactive support to the grid. Some of the DSE results are shown in Fig. 14(b)-(f), and it is noted that CPDSE can effectively track the true states under different sampling frequencies of measurement and control signals. This

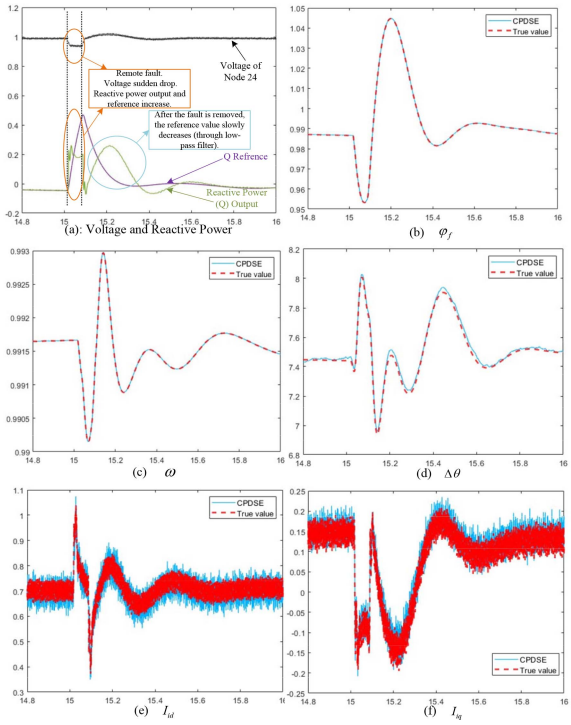


Fig. 15. CPDSE results of a BESS in the IEEE 39-bus test system.

experiment validates the effectiveness of CPDSE for IBRs in the transmission systems.

## V. Conclusion

This paper proposes a fresh DSE framework for the real-time monitoring of IBR dynamics, an increasingly important task in renewable-penentrated power grids. The key difference noted between IBRs and conventional SGs is that IBRs introduce a heavy mix of physical and digital dynamics, and the interaction signals between the two are susceptible to interference and contamination. In order to address this unique challenge, we advocate a control-physics interactive state-space representation of IBRs to address the uncertainty of the two-way data flows between the control and physical subsystems. Therefore, a generic dual CPDSE framework is proposed along with specific models and algorithms to materialize it.

Simulations are first carried out in solar PV systems in the IEEE 13-node test feeder. The numerical results clearly validate the theoretical reflection: under both normal and abnormal operating conditions, the proposed CPDSE framework is consistently advantageous over the traditional method based on the widely-used blended state-space model. Subsequently, the versatility of the proposed framework is validated by presenting DSE results of a PMSG-WT connected to the IEEE 34-node test feeder. By assuming that the state estimator does not have the statistical information about the noises, the adaptation feature of the proposed ACKF algorithm is also validated. Finally, the effectiveness of the proposed framework in the transmission network and under different signal sampling frequencies is validated by presenting the DSE results of a BESS connected to the IEEE 39-bus power system.

As an emerging topic, DSE for IBRs requires more in-depth investigation that goes beyond the scope of a single paper. Possible future work under the proposed CPDSE framework include: 1) enhanced estimator design accounting for detailed IBR properties, such as possible control mode switching and specific process/output noise properties due to non-idealities of power electronics; 2) applications of the CPDSE framework such as model calibration, event detection, control and protection for both the physical inverter system and its digital controller.

## References

[1] M. Nehrir et al., "A review of hybrid renewable/alternative energy systems for electric power generation: Configurations, control, and applications," *IEEE Trans. Sustain. Energy*, vol. 2, no. 4, pp. 392–403, Oct. 2011.

[2] Q. Peng, Q. Jiang, Y. Yang, T. Liu, H. Wang, and F. Blaabjerg, "On the stability of power electronics-dominated systems: Challenges and potential solutions," *IEEE Trans. Ind. Appl.*, vol. 55, no. 6, pp. 7657–7670, Nov./Dec. 2019.

[3] Y. Li, Y. Gu, and T. C. Green, "Mapping of dynamics between mechanical and electrical ports in SG-IBR composite grids," *IEEE Trans. Power Syst.*, vol. 37, no. 5, pp. 3423–3433, Sep. 2022.

[4] H. N. V. Pico and B. B. Johnson, "Transient stability assessment of multi-machine multi-converter power systems," *IEEE Trans. Power Syst.*, vol. 34, no. 5, pp. 3504–3514, Sep. 2019.

[5] Y. Gu and T. C. Green, "Power system stability with a high penetration of inverter-based resources," *Proc. IEEE*, vol. 111, no. 7, pp. 832–853, Jul. 2023.

[6] J. C. Quispe and E. Orduña, "Transmission line protection challenges influenced by inverter-based resources: A review," *Protection Control Modern Power Syst.*, vol. 7, no. 1, pp. 1–17, 2022.

[7] Y. Lin et al., "Pathways to the next-generation power system with inverter-based resources: Challenges and recommendations," *IEEE Electrific. Mag.*, vol. 10, no. 1, pp. 10–21, Mar. 2022.

[8] C. Wang, Z. Qin, Y. Hou, and J. Yan, "Multi-area dynamic state estimation with PMU measurements by an equality constrained extended Kalman filter," *IEEE Trans. Smart Grid*, vol. 9, no. 2, pp. 900–910, Mar. 2018.

[9] S. Yu, K. Emami, T. Fernando, H. H. C. Iu, and K. P. Wong, "State estimation of doubly fed induction generator wind turbine in complex power systems," *IEEE Trans. Power Syst.*, vol. 31, no. 6, pp. 4935–4944, Nov. 2016.

[10] S. Yu, T. Fernando, K. Emami, and H. H.-C. Iu, "Dynamic state estimation based control strategy for DFIG wind turbine connected to complex power systems," *IEEE Trans. Power Syst.*, vol. 32, no. 2, pp. 1272–1281, Mar. 2017.

[11] A. Paul, G. Joos, and I. Kamwa, "Decentralized dynamic state estimation of doubly fed induction generator using terminal measurements," in *Proc. IEEE Power Energy Soc. Innov. Smart Grid Technol. Conf.*, 2018, pp. 1–5.

[12] F. Bakhtiari and J. Nazarzadeh, "Optimal estimation and tracking control for variable-speed wind turbine with PMSG," *J. Modern Power Syst. Clean Energy*, vol. 8, no. 1, pp. 159–167, 2019.

[13] S. Afrasiabi, M. Afrasiabi, M. Rastegar, M. Mohammadi, B. Parang, and F. Ferdowsi, "Ensemble Kalman filter based dynamic state estimation of PMSG-based wind turbine," in *Proc. IEEE Texas Power Energy Conf.*, 2019, pp. 1–4.

[14] S. Huang, T. Wang, T. Ji, and M. Jin, "Adaptive cubature Kalman filter based dynamic state estimation for grid-connected photovoltaic system," in *Proc. 4th Int. Conf. Energy, Elect. Power Eng.*, 2021, pp. 570–575.

[15] Y. Li, L. Zhang, K. Lai, and X. Zhang, "Dynamic state estimation method for multiple battery energy storage systems with droop-based consensus control," *Int. J. Elect. Power Energy Syst.*, vol. 134, 2022, Art. no. 107328.

[16] J. Zhao et al., "Roles of dynamic state estimation in power system modeling, monitoring and operation," *IEEE Trans. Power Syst.*, vol. 36, no. 3, pp. 2462–2472, May 2021.

[17] T. Wang, S. Huang, M. Gao, and Z. Wang, "Adaptive extended Kalman filter based dynamic equivalent method of PMSG wind farm cluster," *IEEE Trans. Ind. Appl.*, vol. 57, no. 3, pp. 2908–2917, May/Jun. 2021.

[18] K. Yue, Y. Liu, P. Zhao, B. Wang, M. Fu, and H. Wang, "Dynamic state estimation enabled health indicator for parametric fault detection in switching power converters," *IEEE Access*, vol. 9, pp. 33224–33234, 2021.

[19] S. Yu, L. Zhang, H. H.-C. Lu, T. Fernando, and K. P. Wong, "A DSE-based power system frequency restoration strategy for PV-integrated power systems considering solar irradiance variations," *IEEE Trans. Ind. Informat.*, vol. 13, no. 5, pp. 2511–2518, Oct. 2017.
[20] Y. Liu, S. Choi, A. S. Meliopoulos, R. Fan, L. Sun, and Z. Tan, "Dynamic state estimation enabled preditive inverter control," in *Proc. IEEE Power Energy Soc. Gen. Meeting*, 2016, pp. 1–5.
[21] S. S. Yu, G. Zhang, T. Fernando, and H. H.-C. Iu, "A DSE-based SMC method of sensorless DFIG wind turbines connected to power grids for energy extraction and power quality enhancement," *IEEE Access*, vol. 6, pp. 76596–76605, 2018.
[22] S. Choi and A. P. S. Meliopoulos, "Effective real-time operation and protection scheme of microgrids using distributed dynamic state estimation," *IEEE Trans. Power Del.*, vol. 32, no. 1, pp. 504–514, Feb. 2017.
[23] Y. Liu et al., "Dynamic state estimation for power system control and protection," *IEEE Trans. Power Syst.*, vol. 36, no. 6, pp. 5909–5921, Nov. 2021.
[24] X. Fu et al., "Large-signal stability of grid-forming and grid-following controls in voltage source converter: A comparative study," *IEEE Trans. Power Electron.*, vol. 36, no. 7, pp. 7832–7840, Jul. 2021.
[25] Q.-C. Zhong and G. Weiss, "Synchronverters: Inverters that mimic synchronous generators," *IEEE Trans. Ind. Electron.*, vol. 58, no. 4, pp. 1259–1267, Apr. 2011.
[26] I. Arasaratnam and S. Haykin, "Cubature Kalman filters," *IEEE Trans. Autom. Control*, vol. 54, no. 6, pp. 1254–1269, Jun. 2009.
[27] A. Sharma, S. C. Srivastava, and S. Chakrabarti, "A cubature Kalman filter based power system dynamic state estimator," *IEEE Trans. Instrum. Meas.*, vol. 66, no. 8, pp. 2036–2045, Aug. 2017.
[28] M. A. Kardan et al., "Improved stabilization of nonlinear DC microgrids: Cubature Kalman filter approach," *IEEE Trans. Ind. Appl.*, vol. 54, no. 5, pp. 5104–5112, Sep./Oct. 2018.
[29] Y. Lin and A. Abur, "A highly efficient bad data identification approach for very large scale power systems," *IEEE Trans. Power Syst.*, vol. 33, no. 6, pp. 5979–5989, Nov. 2018.
[30] R. Mehra, "Approaches to adaptive filtering," *IEEE Trans. Autom. Control*, vol. AC-17, no. 5, pp. 693–698, Oct. 1972.
[31] L. Ling, D. Sun, X. Yu, and R. Huang, "State of charge estimation of lithium-ion batteries based on the probabilistic fusion of two kinds of cubature kalman filters," *J. Energy Storage*, vol. 43, 2021, Art. no. 103070.
[32] *IEEE Standard for Interconnection and Interoperability of Distributed Energy Resources with Associated Electric Power Systems Interfaces*, IEEE Standard 1547–2018, 2018.

**Heqing Huang** (Student Member, IEEE) received the bachelor's and master degrees in electrical engineering from Tsinghua University, Beijing, China, in 2012 and 2015, respectively. He is currently working toward the Ph.D. degree with the Department of Electrical and Computer Engineering, New York University, New York, NY, USA. He was a Research and Development Engineer with NR Electric Company, Ltd from 2015 to 2021, primarily responsible for the R&D of static frequency converters. His research interests include data-driven modeling and dynamic state estimation of smart grids.

**Yuzhang Lin** (Member, IEEE) received the bachelor and master degrees in electrical engineering from Tsinghua University, Beijing, China, in 2012 and 2014, respectively, and the Ph.D. degree in electrical engineering from Northeastern University, Boston, MA, USA, in 2018. He is currently an Assistant Professor with the Department of Electrical and Computer Engineering, New York University, New York, NY, USA. He was an Assistant Professor with the University of Massachusetts, Lowell, MA, USA, prior to joining NYU. His research interests include modeling, situational awareness, data analytics, and cyber-physical resilience of smart grids. He is the Co-Chair of the IEEE PES Task Force on Standard Test Cases of Power System State Estimation, and the Secretary of IEEE PES Distribution System Operation and Planning Subcommittee. He was the recipient of the NSF CAREER Award.

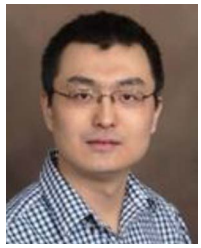

**Xiaonan Lu** (Senior Member, IEEE) received the B.E. and Ph.D. degrees in electrical engineering from Tsinghua University, Beijing, China, in 2008 and 2013, respectively. From 2010 to 2011, he was a guest Ph.D. student with the Department of Energy Technology, Aalborg University, Aalborg, Denmark. From 2013 to 2014, he was a Postdoctoral Research Associate with the Department of Electrical Engineering and Computer Science, University of Tennessee, Knoxville, TN, USA. From 2015 to 2018, he was with the Energy Systems Division, Argonne National Laboratory, first as a Postdoctoral Appointee and then as an Energy Systems Scientist. From 2018 to 2022, he was with the College of Engineering, Temple University, Philadelphia, PA, USA, as an Assistant Professor. In 2022, he joined the School of Engineering Technology with Purdue University, West Lafayette, IN, USA, as an Associate Professor. His research interests include modeling, control and design of power electronic inverters, hybrid AC and DC microgrids, and real-time hardware-in-the-loop simulation. Dr. Lu is an Associate Editor for the IEEE TRANSACTIONS ON INDUSTRIAL ELECTRONICS, IEEE TRANSACTIONS ON INDUSTRY APPLICATIONS, the Editor of IEEE TRANSACTIONS ON SMART GRID, and Editor of *Power Engineering Letters*. He is the Chair of the Industrial Power Converters Committee (IPCC) in the IEEE Industry Applications Society (IAS). He was also the recipient of the 2020 Young Engineer of the Year Award in the IEEE Philadelphia Section.

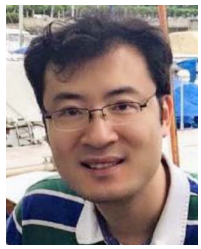

**Yue Zhao** (Member, IEEE) received the B.E. degree in electronic engineering from Tsinghua University, Beijing, China, in 2006, and the Ph.D. degree in electrical engineering from the University of California, Los Angeles, CA, USA, in 2011. He is also an Associate Professor of electrical and computer engineering with Stony Brook University, Stony Brook, NY, USA. His research interests include machine learning, optimization, and game theory with applications in power systems, electricity markets, and grid integration of renewable energies and distributed energy resources.

**Avinash Kumar** (Member, IEEE) received the Ph.D. degree in electrical engineering from the Indian Institute of Technology Kanpur, Kanpur, India, in 2021. He is currently a Postdoctoral Research Associate with the Department of Electrical and Computer Engineering, Virginia Tech, Blacksburg, VA, USA. Before that, he was a Postdoctoral Research Associate with the Department of Electrical and Computer Engineering, University of Massachusetts, Lowell, MA, USA, from 2022 to 2023. His research interests include renewable integration in microgrids, microgrid resiliency, dynamic state estimation, intelligent grids, microgrid protection and control, and ancillary service in distribution networks.